Environ Sci Pollut Res (2017) 24:5991–6001
DOI 10.1007/s11356-016-6692-3

Synthesis and characterization of catalysts based on mesoporous silica partially hydrophobized for technological applications

Amanda R. Martins[1] · **Adriana B. Salviano**[1] · **Aline A. S. Oliveira**[1] · **Raquel V. Mambrini**[2] · **Flávia C. C. Moura**[1]

Received: 22 December 2015 / Accepted: 12 April 2016 / Published online: 22 April 2016

Abstract In this work, mesoporous silica mobil composition of matter no. 41 (MCM-41) was synthesized by the sol-gel method. Two different surface modifications were made to transform this material into a very active adsorbent and catalyst support: (i) impregnation of iron nanoparticles and (ii) hydrophobization via chemical vapor deposition (CVD) with ethanol. The materials prepared with different iron contents, i.e., 2.5, 5, and 10 %, after hydrophobization, were characterized by several techniques. CHN analysis and Raman spectroscopy proved that approximately 15 % of carbon is deposited during CVD process mainly as organized carbonaceous structures. The specific surface area was determined by the BET method as up to 1080 $m^2\ g^{-1}$, which explains the excellent results of the materials in the adsorption of model dyes methylene blue and indigo carmine. Mössbauer spectroscopy, thermogravimetric (TG)/DTG analysis, and transmission electron microscopy (TEM) images showed that the iron supported may be partially reduced during the CVD process to Fe^{2+} species, which are stabilized by the carbon coating. This iron species plays an important role in the oxidation of different contaminants, such as quinoline and methylene blue. The results obtained in the catalytic tests showed to be very promising.

Responsible editor: Santiago V. Luis

✉ Flávia C. C. Moura
flaviamoura@ufmg.br

[1] Departamento de Química, ICEx, Universidade Federal de Minas Gerais, Av. Antônio Carlos, 6627, Pampulha, Belo Horizonte, MG, Brazil CEP 31270-901

[2] Centro Federal de Educação Tecnológica de Minas Gerais, Av. Amazonas 5253, Nova Suíça, Belo Horizonte, MG CEP 30421-169, Brazil

Keywords MCM-41 · Hydrophobization · Carbon · CVD · Supported iron · Adsorption · Oxidation · Fenton · Mesoporous material · Heterogeneous catalysis

Introduction

Mesoporous materials are those formed by pores with a diameter between 20 and 500 Å, according to IUPAC (El-Sharkawy et al. 2007; Pizarro et al. 2015). However, due to the limitation of analytical techniques of that time, the authors were not able to recognize the remarkable features of its products. In 1992, the introduction of micellar aggregates as structural driver agents enabled the synthesis of a new family of mesoporous silica and aluminosilicate compounds, named as M41S. The M41S family of materials consists of three basic members: mobil composition of matter no. 41 (MCM-41) having hexagonal phase, MCM-48 having cubic phase, and MCM-50 material of lamellar phase with poor stability (Vartuli et al. 1994). The porous materials usually present high thermal, hydrothermal, and mechanical stability. Moreover, these materials have a wide application as catalysts and adsorbents, mainly due to its porosity associated with high surface area (Pal and Bhaumik 2013).

The molecular sieve MCM-41 is one of the most studied porous materials. This silica has an arrangement of hexagonal channel of unidirectional, uniform, and not interconnected pores. This material presents some interesting features to adsorptive and catalytic applications, such as (i) well-defined pores with a narrow size distribution (between 1.5 and 10 nm), (ii) possibility of adjusting the pore size, (iii) large pore volume (more than 1 cm^3), (iv) high surface area (700–1500 $m^2\ g^{-1}$), (v) high density of internal silanol groups (40–60 %) with passive surface for modification, and (vi) good thermal, hydrothermal, mechanical, and acidity stability (Li

et al. 2015; Qin et al. 2015). Furthermore, this material can be prepared from a variety of experimental conditions by varying pH, concentration, composition, temperature, and synthesis time.

Different mesoporous materials have been synthesized by the sol-gel method. Some works show (Kresge et al. 1992; Putz et al. 2015) that it is possible to obtain homogeneous materials with great purity at low temperatures using driver agents. The role of surfactant is critical to the formation of the M41S materials. When in aqueous solution, these drivers form micelle agents, around which occurs the condensation of the inorganic precursor. For this, it is necessary that the surfactant molecules be in a sufficient concentration to form a liquid crystal structure. Loads of this surfactant added is balanced by inorganic anions of silicates. Finally, the driver is removed by calcination resulting in a mesoporous material with high specific area (Voss 1999).

The degradation of effluents from the dyeing process is one of the main problems of the textile industry, not only because the criteria for color removal in effluents on the aquatic environment are increasingly demanding but also because their removal is essential for the water reuse in the industrial process.

Another important class of contaminants is that from petroleum-derived liquid fuels such as nitrogenous contaminants. Quinoline is a major nitrogenous organic contaminants present in the oil and its derivatives. The presence of nitrogen compounds adversely influences the stability of fuel and increase water retention even further; its combustion produces harmful air pollutants and precursor species of acid rain. Thus, the removal of these contaminants has remarkable economic and environmental relevance (Mambrini et al. 2013).

Several waste treatment techniques have been developed, such as absorption and filtration (Gad and El-Sayed 2009), biological degradation (Paździor et al. 2009), and advanced oxidation processes (AOPs) (Rahim Pouran et al. 2015). AOPs are one of the most promising technologies to degrade aromatic organic compounds with high molecular stability. The AOPs are physico-chemical processes based on the in situ generation of intermediate species able to promote the oxidation and/or mineralization of toxic organic compounds. Among the AOPs, Fenton-like reactions are the most promising. The Fenton mechanism is based on the generation of hydroxyl radical (•OH) from hydrogen peroxide (H_2O_2), catalyzed by iron(II) ions, and has been widely explored in the oxidation of organic compounds, especially textile dyes and contaminants from liquid fuels (Borràs et al. 2013; Martins et al. 2015; Rahim Pouran et al. 2015; Teixeira et al. 2012) (Fig. 1).

As far as we know, this is the first time that materials combining MCM-41 matrix, Fe supported on their surface and partial carbon coating are applied in adsorption and oxidation of quinoline and/or organic dyes.

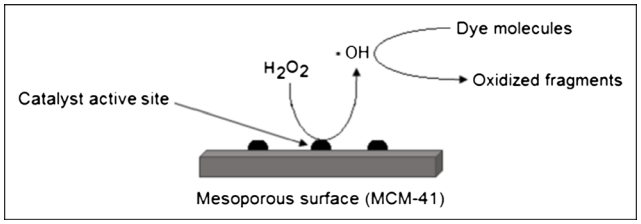

Fig. 1 Schematic representation of Fenton process catalyzed by metal nuclei on MCM-41

Experimental

Synthesis of MCM-41

The synthesis of MCM-41 was based on a modification of the synthesis described by Grün et al. (Grün et al. 1999), in which the cetyltrimethylammonium bromide (CTAB) was used as surfactant, tetraethylorthosilicate (TEOS) as silica source, sodium hydroxide (NaOH) as catalyst, and deionized water as solvent. These reactants were added in accordance with the following molar ratio: 0.12 CTAB/1 TEOS/0.6 NaOH/100 H_2O.

The synthesis involved the following steps: (a) dissolution of the CTAB in aqueous NaOH (1 mol L^{-1}); (b) adding the TEOS under stirring at room temperature; (c) washing the resulting material with milli-Q water; (d) drying the solid (MCM-41 precursor) for 12 h at 60 °C; (e) calcination of this precursor at 550 °C for 6 h under air flow, thereby obtaining MCM-41.

Modifications on MCM-41

Two groups of materials were prepared by different surface modifications: (i) iron impregnation and (ii) carbon deposition. Iron was used as metal catalyst and was supported by wet impregnation on MCM-41 in different mass ratios, i.e., 2.5, 5.0, or 10.0 %. An alcoholic solution of $FeCl_3 \cdot 6H_2O$ salt (Synth) was added to the MCM-41 dispersion, and the system was left under stirring for 24 h for complete evaporation of the solvent. The solid obtained was calcined at 300 °C for 60 min under air flow. The materials were named by their iron content: MCM41/Fe2.5, MCM41/Fe5, and MCM41/Fe10.

These materials impregnated with different proportions of Fe underwent a hydrophobization process for carbon deposition on their surface. The carbon deposition should increase the hydrophobic character of the materials, as well as stabilize the iron particles on the materials' surface and increase the formation of active species that favors the adsorption (Calvete et al. 2010; Purceno et al. 2011) and oxidation processes (Lima et al. 2008). The hydrophobized materials were named according to the iron content, MCM41/Fe2.5/C, MCM41/Fe5/C, and MCM41/Fe10/C. The hydrophobization were performed via chemical vapor deposition (CVD) process

(Manikandan et al. 2013), using ethanol as carbon source. The carbon deposition occurred in a reactor consisting of a quartz tube in a tubular furnace. The materials impregnated with iron were heated to 700 °C at 10 °C min^{-1} under ethanol/N_2 flow of 50.0 mL min^{-1}.

Carbon deposits were produced from ethanol decomposition. The thermal decomposition of ethanol occurs typically above 650 °C but iron nuclei reduce this temperature, since they act in the dehydrogenation of ethanol and in the nucleation and growth of carbon nanostructures (Oliveira et al. 2011; Pinilla et al. 2011).

Characterization of the materials

The materials were characterized by a variety of techniques: CHN elemental analysis (Perkin-Elmer-Séries II-CHNS/O Analyzer 2400, with a combustion chamber temperature near to 926 °C), thermogravimetric (TG) analysis (in air flow, 100 mL min^{-1}, heating rate of 10 °C min^{-1} up to 900 °C in an DTG-60 Shimadzu), Mössbauer spectroscopy (room temperature in a spectrophotometer CMTE MA250, with constant acceleration, Co source, Rh matrix, and α-Fe as reference), transmission electron microscopy coupled with energy-dispersive spectroscopy (TEM and EDS) (microscope Tecnai G2-20-SuperTwin FEI-200 kV, samples dispersed in acetone and deposited on a Cu screen), Raman spectroscopy (Bruker spectrometer SENTERRA, equipped with a CCD detector, using a laser with $\lambda = 633$ nm), specific surface area and porosity—N_2 adsorption/desorption (Autosorb-1MP equipment, Quantachrome Instruments Corp. at −196 °C, samples previously degasified at 150 °C for 8 h), and zeta potential at different pHs (ZetaSiker equipment, Malvern Instruments—with composites dispersed in deionized water).

Application of the materials

Dye adsorption tests were carried out using methylene blue (MB) as a cationic molecule model and indigo carmine (IC) as anionic molecule model (IC). The adsorption experiments were performed with 10.0 mL of a 100.0 mg L^{-1} MB solution and 20.0 mg of the materials (adsorbents). Adsorption of the dyes was monitored by the MB or IC decolorization using a UV-vis spectrophotometer 2550—Shimadzu at 664 and 365 nm wavelengths, respectively. Adsorption of methylene blue and indigo carmine was carried out using a calibration curve in the range of 10–200 ppm of each dye in water. During the adsorption tests, the absorbance of the dyes was compared to absorbance values of the standard solutions in the calibration curve. The adsorption promoted by the materials was determined by the difference between the initial concentration of the solution and the concentration determined after contact between the adsorbent and the dye solution.

The catalytic activity of the materials produced was evaluated in the oxidation of MB in an aqueous medium, using 1.0 mL of hydrogen peroxide as oxidizing agent, 10.0 mL of a 30.0 mg L^{-1} dye solution, and 20.0 mg of material. Initially, the adsorption effect was eliminated during a 24-h contact of the materials to a 500.0 mg L^{-1} dye solution. Then, these materials were filtered off and, only after drying, were used in oxidation reactions. The oxidation was monitored by discoloration of the solutions using an UV-vis spectrophotometer 2550—Shimadzu ($\lambda = 664$ nm).

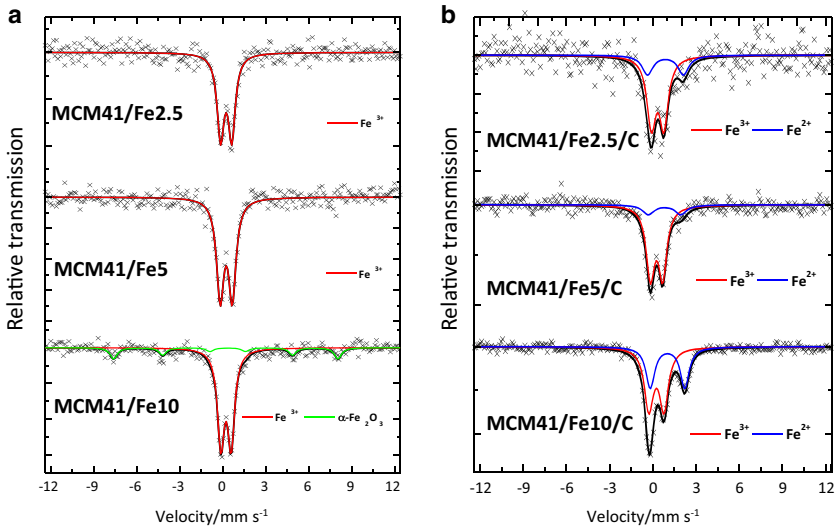

Fig. 2 ^{57}Fe room temperature Mössbauer spectra of MCM-41-based materials: **a** after iron impregnation and **b** after carbon deposition materials

Table 1 Mössbauer hyperfine parameters determined for iron phases in MCM41/Fe and MCM41/Fe/C samples

	Phases	ε (mms^{-1}) (±0.05)	Δ/2ξq (mms^{-1}) (±0.05)	B_{HF} (T) (±0.2)	Area (%) (±1)
MCM41/Fe2.5	Fe^{3+}	0.34	0.77	–	100
MCM41/Fe5	Fe^{3+}	0.35	0.84	–	100
MCM41/Fe10	Fe^{3+}	0.34	0.73	–	80
	α-Fe_2O_3	0.36	−0.14	48.9	20
MCM41/Fe2.5/C	Fe^{3+}	0.39	0.77	–	74
	Fe^{2+}	0.97	2.48	–	26
MCM41/Fe5/C	Fe^{3+}	0.36	0.84	–	84
	Fe^{2+}	1.02	2.39	–	16
MCM41/Fe10/C	Fe^{3+}	0.36	1.04	–	60
	Fe^{2+}	1.02	2.39	–	40

δ α-Fe relative isomeric shift, ε quadrupole shift, Δ quadrupole splitting, *Bhf* hyperfine magnetic field

The nitrogen oxidation tests were performed using the quinoline as a model molecule. Initially, the materials were left in contact with a quinoline solution (500.0 mg L^{-1} of nitrogen) for 24 h so that the effect of adsorption was eliminated. After filtered and dried, the materials were used in oxidation reactions.

The procedures were carried out using 10.0 mL of a 30.0 mg L^{-1} of quinoline solution, 1.0 mL of oxidation mixture (1 H_2O_2/1 HCOOH), and 30.0 mg of the material. The quinoline oxidation reactions were followed by mass spectrometry with electrospray ionization—Thermo LCQ Fleet.

Results and discussion

Characterization of the materials

The materials based on MCM-41 were first characterized with respect to the iron phases by Mössbauer spectroscopy (Fig. 2). The hyperfine parameters used for phase identifications are shown in Table 1.

The iron impregnation was prepared with $FeCl_3$ salt, which means that all iron was supported as Fe^{3+}. It is observed that after CVD process, part of the iron present on MCM-41 is reduced to Fe^{2+}, i.e., 26, 16, and 40 % of Fe^{2+} on MCM41/Fe2.5/C, MCM41/Fe5/C, and MCM41/Fe10/C, respectively. In addition, we may infer that the iron is supported as very small particles without expressive formation of well-defined phases, such as iron silicate or iron oxide. Only the material with 10 % of iron was capable of producing a well-defined phase, α-Fe_2O_3, with 20 % of relative area (Table 1).

The sample MCM41/Fe2.5/C has shown a greater concentration of reduced iron in relation to the sample MCM41/Fe5/C. This behavior may be related to the formation of iron particles slightly larger in the sample MCM41/Fe5/C with lower availability of metal sites on the surface of this material compared to MCM41/Fe2.5/C. The sample MCM41/Fe10/C showed a greater content of Fe^{2+}, as expected, due to its higher iron content.

The CHN elemental analysis was carried out to determine the carbon content in the composition of the materials. It was found that MCM41/Fe2.5/C, MCM41/Fe5/C, and MCM41/Fe10/C present 12, 13, and 15 % C, respectively. The carbon content is enhanced in materials with more iron; however, this increase cannot be linearly related to the iron content.

TG experiments were conducted to study the thermal behavior of the samples and to verify the efficiency of the CVD process on the carbon formation. The thermogravimetric

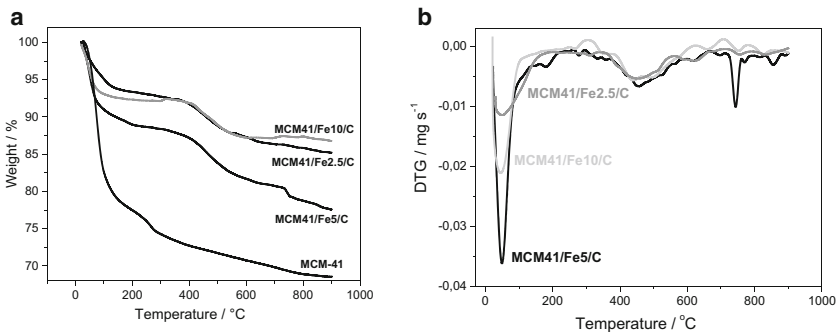

Fig. 3 **a** TG profiles obtained for pure MCM-41 and carbon composites, under air atmosphere, and **b** DTG curves for MCM41/Fe2.5/C, MCM41/Fe5/C, and MCM41/Fe10/C

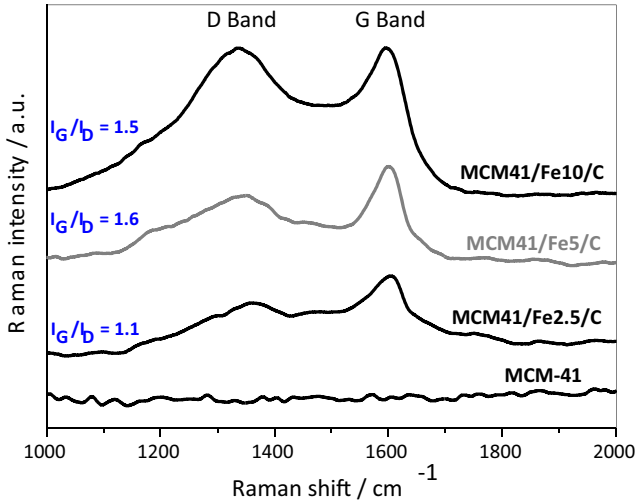

Fig. 4 Raman spectra ($\lambda = 633$ nm) obtained for samples MCM-41 and MCM41/Fe/C series

curves for pure MCM-41 and for carbon materials MCM41/Fe/C are shown in Fig. 3.

Two events of weight loss can be seen in the TG profile of pure MCM-41: The first one, before 100 °C, related to surface water desorption (~5 %), and the second event at 150–350 °C associated with the dehydroxylation of silanol groups (around 20 %). For the materials prepared after CVD, the TG profiles also show the water desorption before 100 °C. For the materials with carbon, it was possible to observe that a weight loss from 300 °C related two simultaneous events. According to Mössbauer results, the catalysts prepared by CVD present Fe^{2+} species, which can be oxidized to form Fe_2O_3, resulting in a TG weight gain. Simultaneously, the carbon present in the materials can be oxidized to form CO and CO_2, resulting a weight loss between 400 and 600 °C. Since the amount of carbon deposited on the material is higher than the amount of iron, the weight loss event is evidenced.

Regarding the derivative of TG profiles (DTG curves—Fig. 3b), the curves obtained for all the materials produced show the isothermic peak for water dessorption centered at 50 °C. Moreover, only in the profile of MCM41/Fe5/C sample is observed a fairly sharp and intense peak at 750 °C, which might be related to the burn off of organized carbon structure, such as graphitic carbon. Graphite is more stable than a defected carbon, which should be oxidized at lower temperatures, for example, 350–550 °C (Nxumalo et al. 2010).

In Fig. 4, the Raman spectra obtained for the series of MCM41/Fe/C materials are shown. Raman spectroscopy is important to characterize the quality of the carbonaceous structures produced on the surface of the materials. Different carbon structures exhibit characteristic vibrational modes that may be identified in different regions of a Raman spectrum (Dresselhaus et al. 2008).

In the frequency region between 1500 and 1600 cm^{-1} of Raman spectra (Fig. 4), we may see the G band, mainly related to a vibrational mode characteristic of organized graphitic carbon. This vibrational mode is caused by the tangential vibration of two carbon atoms, one against the other, in organized structures (Dresselhaus et al. 2008). On the other hand, defective or disorganized carbon is identified by the D band that is typically between 1300 and 1400 cm^{-1}. Pure support MCM-41 and iron phases present no bands in the frequency region analyzed, so we may infer that all bands observed in the spectra obtained are due to the carbon deposits. It is observed that G band is narrower than D, also more intense and better defined as the Fe content increases.

The ratio of the relative intensities of G and D bands (I_G/I_D) can be analyzed as a measure of the carbon structures' organization/quality (Oliveira et al. 2013a; Wang et al. 2015). The I_G/I_D ratio calculated for MCM41/Fe2.5/C, MCM41/Fe5/C, and MCM41/Fe10/C are 1.1, 1.6, and 1.5, respectively. These values indicate that the amount of graphitic carbon formed on the materials is greater than the amount of disorganized/defective carbon in all materials. Even if the MCM41/Fe10/C material gives the largest amount of carbon deposited, this material does not have the highest I_G/I_D ratio, because when the iron content is much higher, it is harder to control carbon growth.

The structure of the materials was studied by TEM. All materials of the series MCM41/Fe/C show similar TEM images, as represented by MCM41/Fe10/C in Fig. 5. In general, it was observed that the MCM-41 support presents slightly organized and porous structure (Fig. 5a). In the materials

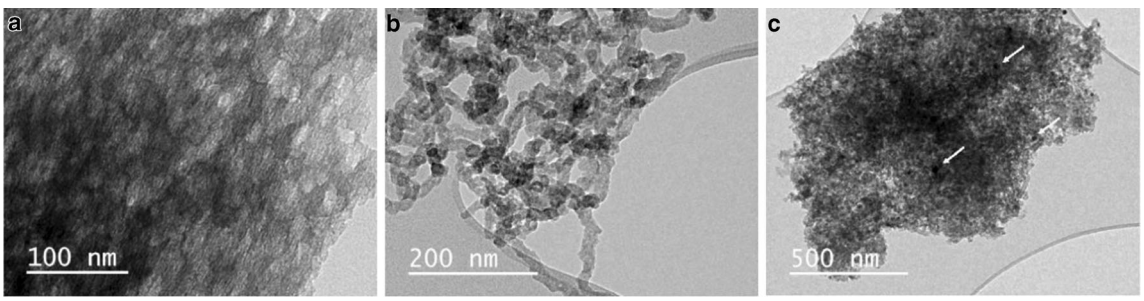

Fig. 5 TEM images obtained for the material MCM41/Fe10/C

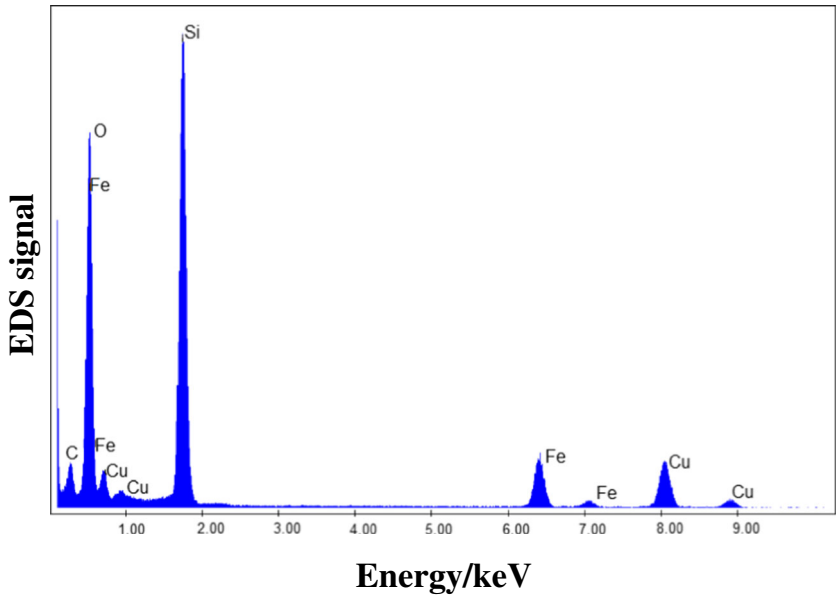

Fig. 6 EDS spectrum of MCM41/Fe10/C material

prepared after Fe impregnation and CVD with ethanol, some twisted filaments can be seen with diameters of approximately 30 nm (Fig. 5b). Metallic and dense particles may also be observed in TEM images, likely supported iron nanoparticles (Fig. 5c).

EDS spectra were obtained from the TEM images. The EDS microanalysis of MCM41/Fe10/C (Fig. 6) indicates a more intense peak on silica beyond the presence of iron and carbon as expected. The signal of cupper is found due to the sample port of the equipment. The EDS spectra confirmed an oxidation of ethanol by the presence of iron in the MCM-41, forming carbon.

The N_2 adsorption/desorption isotherms and the BJH pore size distribution are shown in Fig. 7.

The isotherms shown in Fig. 7a are type IV, exhibiting a hysteresis for p/p_0 close to 0.40, characteristic of mesoporous materials (El-Sharkawy et al. 2007; Luan et al. 1995). The hysteresis of type IV exhibits a loop, i.e., the adsorption and desorption isotherms do not coincide over a certain region of external pressures (Sing et al. 2008). At low pressures, first, an adsorbate monolayer is formed on the pore surface, which is followed by the multilayer formation. The point $p/p_0 = 0.4$ indicates the stage at which the monolayer coverage is complete. In the range of 0.0–0.4 p/p_0, the surface area is determined by the BET method.

From Fig. 7b, we may see that the average pore diameter of pure MCM-41 and hydrophobized materials is approximately 40 Å, and it does not change after CVD reaction. It can be observed in Table 2 that all materials produced present a high specific surface area, especially MCM-41. However, the materials present a decrease in the surface area and pore volume from pure support. This decrease might be related to the

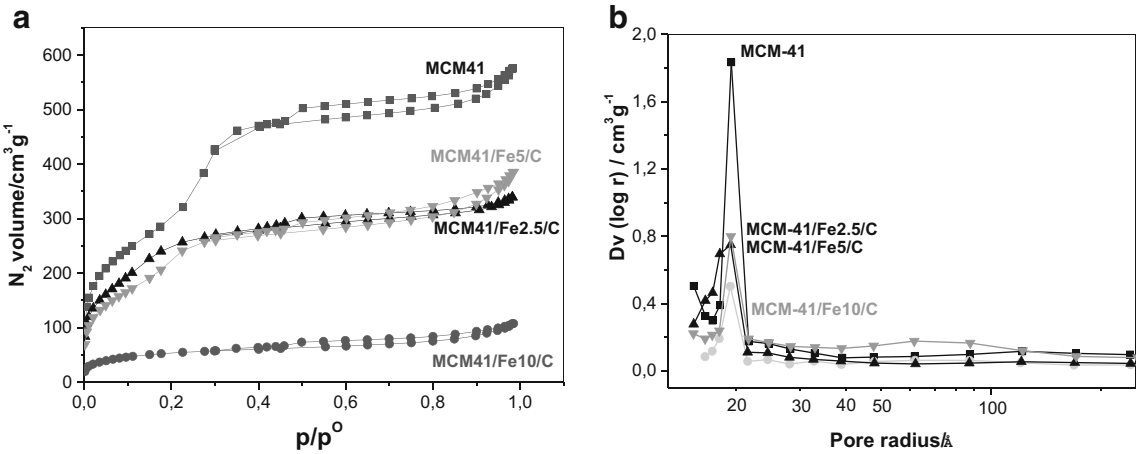

Fig. 7 **a** N_2 adsorption/desorption isotherms and **b** pore size distribution for pure MCM-41 and hydrophobized materials

Table 2 Specific surface area of the materials studied determined by the BET method

Material	Specific surface area ($m^2\ g^{-1}$)	Total pore volume ($cm\ g^{-1}$)
MCM-41	1080	0.890
MCM41/Fe2.5/C	941	0.525
MCM41/Fe5/C	775	0.596
MCM41/Fe10/C	201	0.166

occupation of MCM-41 pores by iron nanoparticles and carbon structures produced during CVD process. Furthermore, the thermal treatment can also contribute to these decreases in the specific surface area and pore volume by destroying some pores, although according to Chen and coworkers (Chen et al. 1993), pure silica MCM-41 can be heated to at least 850 °C before its structure collapses. The CVD process was conducted at 700 °C because it is known that ethanol decomposition at this temperature leads to carbon deposition as organized structures on the surface of the matrix (Oliveira et al. 2011).

Application of the materials

The adsorption kinetic of the MCM-41-based materials was investigated using MB and IC dyes. The behavior of each material for dye adsorption is shown in Fig. 8.

It can be seen in Fig. 8a that over 180 min, the materials prepared reach 79, 74, 88, and 94 % of MB removal for MCM-41, MCM41/Fe2.5/C, MCM41/Fe5/C, and MCM41/Fe10/C, respectively. Pure MCM-41 is a good adsorbent for MB, since it removes 79 % within 180 min of contact. This is likely related to the high specific surface area of this material, i.e., 1080 $m^2\ g^{-1}$. However, it is observed that materials prepared with 5 and 10 % of iron and carbon exhibit higher activities than pure MCM-41, up to 88 and 94 %, even though they present lower surface areas, i.e., 775 and 201 $m^2\ g^{-1}$.

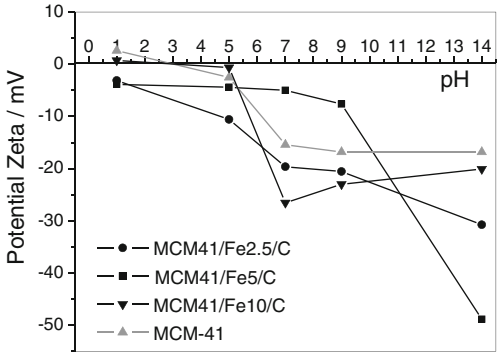

Fig. 9 Zeta potential measurements for MCM-41 and hydrophobized materials obtained after ethanol/CVD process at 800 °C

Therefore, the adsorption process is not related only to the physical morphology of the materials but also to a chemical component. It seems that the greater the iron and carbon content on the adsorbent, the more MB is removed from the liquid phase. It is proposed that the carbonaceous structures on the surface of the materials favor adsorption since they interact better with the nonpolar portion of the dye molecule (Oliveira et al. 2015).

Figure 8b shows the adsorption of indigo carmine (a negatively charged molecule) for the series of MCM41/Fe/C materials. According to data of Fig. 8b, the materials MCM-41, MCM41/Fe2.5/C, MCM41/5Fe/C, and MCM41/Fe10/C adsorb 5, 21, 18, and 13 % of the dye in 180 min, respectively. The dye adsorption capacity does not follow the increase on surface area or even the porosity (pore volume and size), so the adsorption of this series of materials should also be influenced by other factors, such as the charge generated on their surface in aqueous media and the availability of adsorption centers. Therefore, the iron species and the carbon structures might contribute to those main changes on the surface of the materials, thus increasing the methylene blue adsorption. Moreover, it is observed that the adsorption capacity is

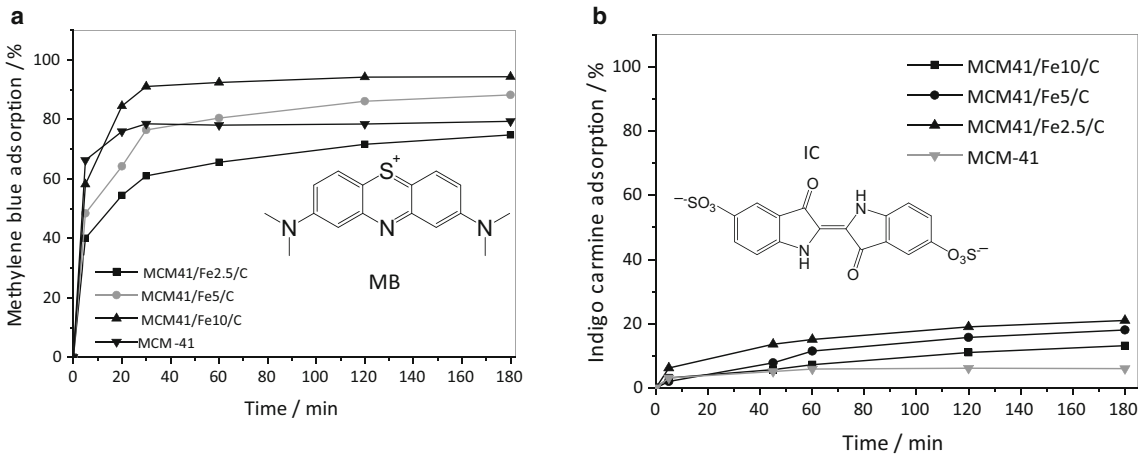

Fig. 8 Adsorption monitoring of **a** methylene blue and **b** indigo carmine, by the MCM-41 and hydrophobized materials

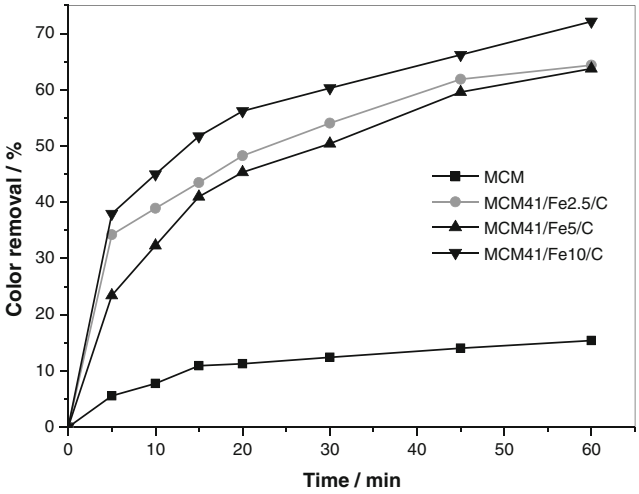

Fig. 10 Methylene blue discoloration catalyzed by the MCM-41-based materials

inversely proportional to the amount of metal supported, so this metal is expected to generate negative charges that repel the anionic molecules of IC, which corroborates the results for the adsorption of methylene blue dye (cationic dye—Fig. 8). These results suggest that surface charges generated on the materials in aqueous medium may be significantly contributing to the adsorption results observed for the different dyes, methylene blue (cationic) and indigo carmine (anionic) (Mambrini et al. 2012).

In order to understand these electrostatic interactions between the dyes and the hidrophobized materials, zeta potential measurements at different pH were carried out (Fig. 9). The zeta potential at different pH curves allows the determination of the point of zero charge (PZC) of the materials and an evaluation of the surface charge of the particles under study.

Figure 9 shows a PZC at pH 3 for the MCM-41 and MCM41/Fe10/C materials. The MCM41/Fe2.5/C and MCM41/Fe5/C materials presented negatively charged throughout the pH range. Since the initial pH of the dye solutions was 7.0, those results indicated that the surface of the materials is negatively charged and therefore preferentially adsorb positively charged molecules such as methylene blue dye. The MCM41/Fe10/C material has lower specific area, but the highest negative charge value at pH 7, which justifies the higher adsorption of methylene blue for this material. On the other hand, the materials negatively charged showed very low adsorption for the negative IC.

The materials were also tested as catalysts for the methylene blue oxidation reaction with H_2O_2. In this case, the adsorption effect was previously eliminated during a 24-h contact of the materials to a very concentrated solution of the dye, i.e., 500.0 mg L^{-1}. These materials were then filtered, dried, and used in a fresh MB solution for the oxidation reactions. After addition of hydrogen peroxide, it is observed (Fig. 10) that the MCM-41 promotes low color removal, approximately 15 % after 60 min. On the other hand, MCM41/Fe2.5/C, MCM41/Fe5/C, and MCM41/Fe10/C remove in 60 min 64, 63, and 72 %, respectively. Similar materials have reached lower activities in the same experimental conditions (Rahim Pouran et al. 2015).

The highest catalytic activity of MCM41/Fe10/C was expected and may be mainly related to two factors: (i) greater amount of carbon on this material in relation to MCM41/Fe5/

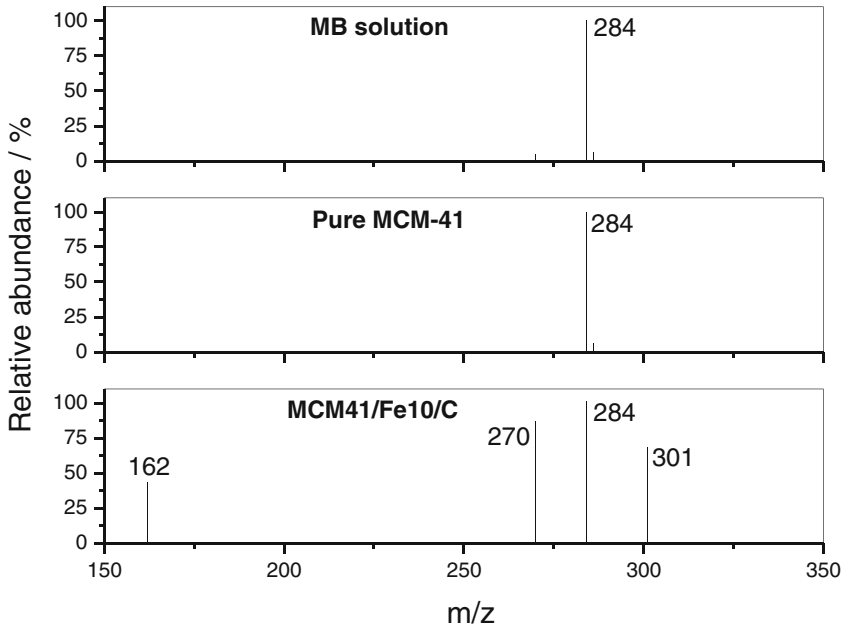

Fig. 11 Monitoring of methylene blue oxidation in the presence of MCM41/Fe10/C catalyst, by ESI-MS

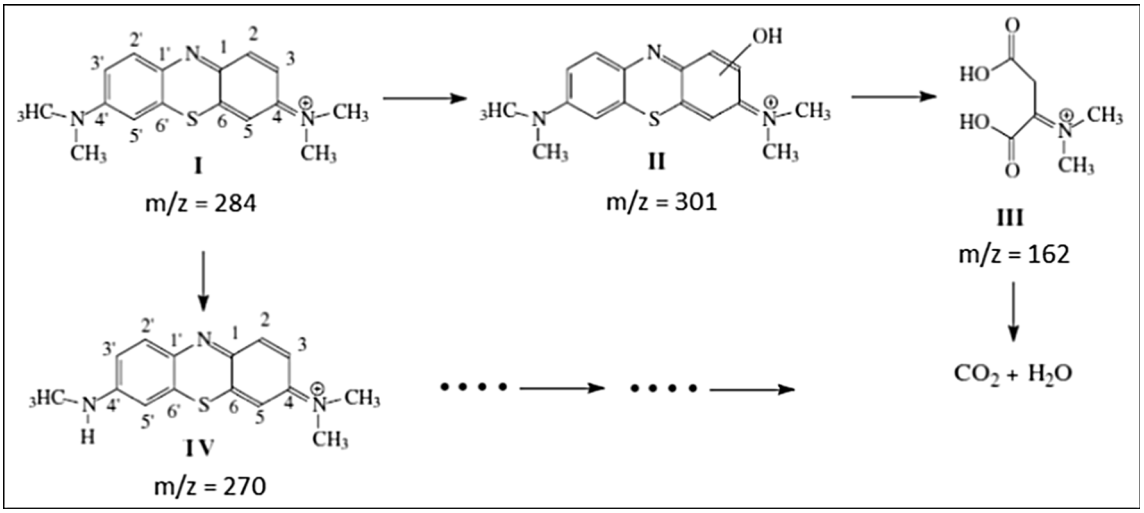

Fig. 12 Intermediates of methylene blue oxidation in the presence of the MCM catalysts

C and MCM41/Fe2.5/C, which facilitates the adsorption of the contaminant on the catalyst surface, and (ii) higher Fe^{2+} content, which is the most active iron phase for oxidation reactions in Fenton-like process.

After 180 min of reaction, the oxidation products were determined by mass spectrometry with electrospray ionization (ESI/MS) (Fig. 11).

From the ESI-MS data, it is observed that methylene blue produces a characteristic signal $m/z = 284$. After 180-min reaction with hydrogen peroxide in the presence of the catalyst MCM41/Fe10/C, new signals are shown in the ESI-MS spectra, i.e., $m/z = 162$, 270, and 301. We suggest that the available iron species dispersed on the surface of the MCM-41 can promote the generation of $^{\bullet}OH$ radicals, favoring the oxidation of the methylene blue molecules. The new peaks observed in the presence of the MCM41/Fe10/C catalyst prove that not only the solution discoloration occurs but also MB (m/z 284) is oxidized in the presence of the material, which does not occur in the presence of pure MCM-41.

In Fig. 12 are shown the proposed initial oxidation mechanism with the structural formulas of the products identified by ESI-MS. The molecule $m/z = 301$ is the product of the dye hydroxylation, while the $m/z = 270$ is related to the loss of a methyl radical, and $m/z = 162$ is the molecule formed due to

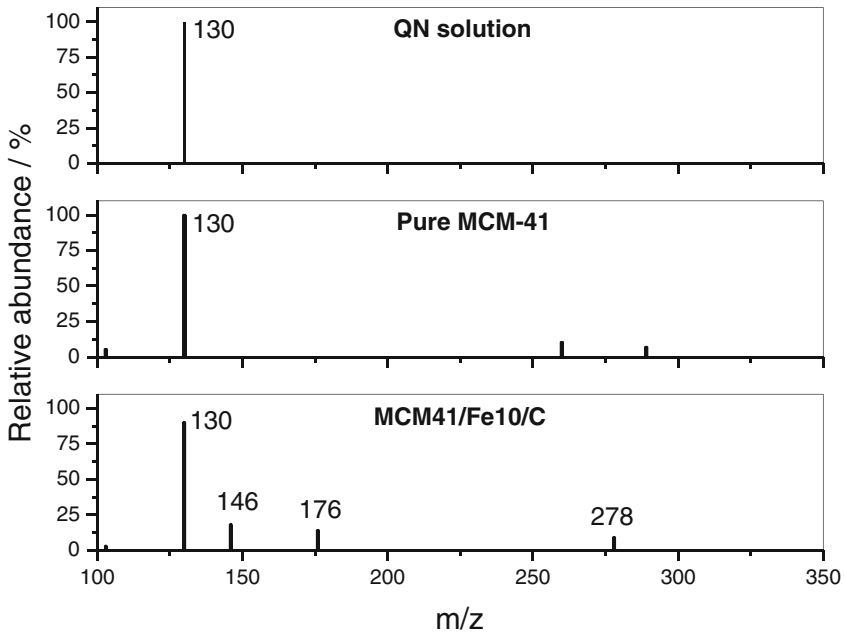

Fig. 13 Monitoring of quinoline oxidation in the presence of MCM41/Fe10/C catalyst, by ESI-MS

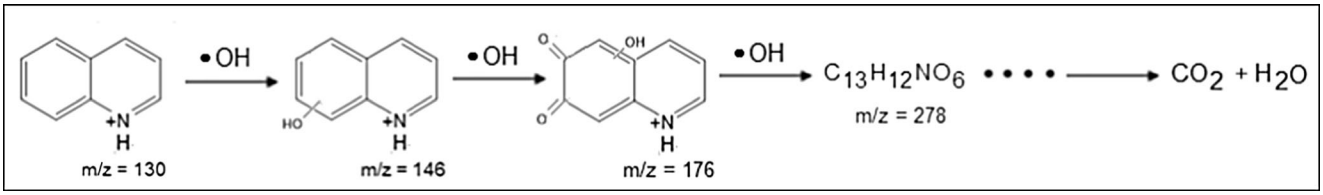

Fig. 14 Intermediates for quinoline oxidation reaction in the presence of the catalyst MCM41/Fe10/C

the break of methylene blue chain (Costa et al. 2015; Esteves et al. 2008).

Quinoline (QN) was tested in the oxidation experiments as model nitrogen contaminant present in liquid fuels. Quinoline oxidation was monitored by ESI-MS after 180 min with hydrogen peroxide in the presence of pure MCM-41 and MCM41/Fe10/C catalyst (Fig. 13).

In ESI-MS results obtained for quinoline, it is observed a rather intense signal ratio $m/z = 130$ corresponding to the protonated quinoline structure. After 180-min reaction, new signals appear in the spectrum only for MCM41/Fe10/C catalyst, i.e., $m/z = 146$, 176, and 278, referring to quinoline oxidation products.

The product with $m/z = 146$ corresponds to the input of the hydroxyl quinoline structure, suggesting the formation of •OH radicals promoted by the decomposition reaction of hydrogen peroxide catalyzed by the material MCM41/Fe10/C. The signal ratio $m/z = 176$ should be related to the oxidation of hydroxyl groups, leading to the formation of ketones. Figure 14 shows a proposal for the formation of possible intermediate of quinoline oxidation reaction. The formation of these oxidized intermediates is reported in the literature by Oliveira et al. and Souza et al. (de Souza et al. 2010; Oliveira et al. 2013b).

Conclusions

Mesoporous silica MCM-41 was produced via sol-gel process and modified by CVD. The surface modifications transformed this material into versatile mesoporous materials with great potential to be used in different technological applications, such as adsorption and catalysis. Iron was first supported on the surface of MCM-41 to catalyze the CVD reaction with ethanol as carbon source. The materials prepared with different iron contents, i.e., 2.5, 5, and 10 % and after partial hydrophobization (12–15 % C), were extensively characterized. The materials have shown to be very active as methylene blue and indigo carmine adsorbents due to their mesoporous structure and high specific surface area, i.e., up to 1080 $m^2\ g^{-1}$. Preliminary studies on the catalysis of dyes and quinoline removal showed very promising results. It was shown that the iron species formed during the hydrophobization process (especially Fe^{2+}) play important roles in the mechanism of these oxidation reactions.

Acknowledgments The authors would like to acknowledge CAPES, CNPq, and FAPEMIG for financial support and the Center of Microscopy at the Universidade Federal de Minas Gerais (http://www.microscopia.ufmg.br) for providing the equipment and technical support for experiments involving electron microscopy.

References

Borràs N, Arias C, Oliver R, Brillas E (2013) Anodic oxidation, electro-Fenton and photoelectro-Fenton degradation of cyanazine using a boron-doped diamond anode and an oxygen-diffusion cathode. J Electroanal Chem 689:158–167. doi:10.1016/j.jelechem.2012.11.012

Calvete T, Lima EC, Cardoso NF, Vaghetti JCP, Dias SLP, Pavan FA (2010) Application of carbon adsorbents prepared from Brazilian-pine fruit shell for the removal of reactive orange 16 from aqueous solution: kinetic, equilibrium, and thermodynamic studies. J Environ Manag 91:1695–1706. doi:10.1016/j.jenvman.2010.03.013

Chen C-Y, Li H-X, Davis ME (1993) Studies on mesoporous materials. Microporous Mater 2:17–26. doi:10.1016/0927-6513(93)80058-3

Costa DAS, Oliveira AAS, de Souza PP, Sapag K, Moura FCC (2015) The combined effect between Co and carbon nanostructures grown on cordierite monoliths for the removal of organic contaminants from the liquid phase. New J Chem 39:1438–1444. doi:10.1039/C4NJ01950D

de Souza WF, Guimarães IR, Oliveira LCA, Giroto AS, Guerreiro MC, Silva CLT (2010) Effect of Ni incorporation into goethite in the catalytic activity for the oxidation of nitrogen compounds in petroleum. Appl Catal A Gen 381:36–41. doi:10.1016/j.apcata.2010.03.036

Dresselhaus MS, Dresselhaus G, Saito R, Jorio A (2008) Raman spectroscopy of carbon nanotubes. In: Elsevier B.V., pp 83–108. doi:10.1016/s1572-0934(08)00004-8

El-Sharkawy EA, Soliman AY, Al-Amer KM (2007) Comparative study for the removal of methylene blue via adsorption and photocatalytic degradation. J Colloid Interface Sci 310:498–508. doi:10.1016/j.jcis.2007.02.013

Esteves A, Oliveira LCA, Ramalho TC, Goncalves M, Anastacio AS, Carvalho HWP (2008) New materials based on modified synthetic Nb2O5 as photocatalyst for oxidation of organic contaminants. Catal Commun 10:330–332. doi:10.1016/j.catcom.2008.09.012

Gad HMH, El-Sayed AA (2009) Activated carbon from agricultural by-products for the removal of Rhodamine-B from aqueous solution. J Hazard Mater 168:1070–1081. doi:10.1016/j.jhazmat.2009.02.155

Grün M, Unger KK, Matsumoto A, Tsutsumi K (1999) Novel pathways for the preparation of mesoporous MCM-41 materials: control of porosity and morphology. Microporous Mesoporous Mater 27:207–216. doi:10.1016/S1387-1811(98)00255-8

Kresge CT, Leonowicz ME, Roth WJ, Vartuli JC, Beck JS (1992) Ordered mesoporous molecular sieves synthesized by a liquid-crystal template mechanism. Nature 359:710–712

Li X, Shi B, Li M, Mao L (2015) Synthesis of highly ordered alkyl-functionalized mesoporous silica by co-condensation method and applications in surface coating with superhydrophilic/antifogging properties. J Porous Mater 22:201–210. doi:10.1007/s10934-014-9886-4

Lima EC et al (2008) Application of Brazilian pine-fruit shell as a biosorbent to removal of reactive red 194 textile dye from aqueous solution: kinetics and equilibrium study. J Hazard Mater 155:536–550. doi:10.1016/j.jhazmat.2007.11.101

Luan Z, He H, Zhou W, Cheng C-F, Klinowski J (1995) Effect of structural aluminium on the mesoporous structure of MCM-41. J Chem Soc Faraday Trans 91:2955–2959. doi:10.1039/FT9959102955

Mambrini RV, Fonseca TL, Dias A, Oliveira LCA, Araujo MH, Moura FCC (2012) Magnetic composites based on metallic nickel and molybdenum carbide: a potential material for pollutants removal. J Hazard Mater 241–242:73–81. doi:10.1016/j.jhazmat.2012.09.002

Mambrini RV, Saldanha ALM, Ardisson JD, Araujo MH, Moura FCC (2013) Adsorption of sulfur and nitrogen compounds on hydrophobic bentonite. Appl Clay Sci 83–84:286–293. doi:10.1016/j.clay.2013.08.030

Manikandan D, Mangalaraja RV, Avila RE, Siddheswaran R, Anathakumar S (2013) Montmorillonite–carbon nanotube nanofillers by acetylene decomposition using catalytic CVD. Appl Clay Sci 71:37–41. doi:10.1016/j.clay.2012.10.001

Martins AS, Vasconcelos VM, Ferreira TCR, Pereira-Filho ER, Lanza MRV (2015) Simultaneous degradation of diuron and hexazinone herbicides by Photo-Fenton: assessment of concentrations of H₂O₂ and Fe²⁺ by the response surface methodology. J Adv Oxid Technol 18:9–14

Nxumalo EN, Letsoalo PJ, Cele LM, Coville NJ (2010) The influence of nitrogen sources on nitrogen doped multi-walled carbon nanotubes. J Organomet Chem 695:2596–2602

Oliveira AAS, Tristao JC, Ardisson JD, Dias A, Lago RM (2011) Production of nanostructured magnetic composites based on Fe0 nuclei coated with carbon nanofibers and nanotubes from red mud waste and ethanol. Appl Catal B 105:163–170. doi:10.1016/j.apcatb.2011.04.007

Oliveira AAS et al (2013a) Magnetic amphiphilic nanocomposites produced via chemical vapor deposition of CH4 on Fe–Mo/nano-Al2O3. Appl Catal A Gen 456:126–134. doi:10.1016/j.apcata.2013.02.027

Oliveira LCA, Fabris JD, Pereira MC (2013b) Óxidos de ferro e suas aplicações em processos catalíticos: uma revisão. Quim Nov. 36:123–130

Oliveira AAS, Christofani T, Teixeira IF, Ardisson JD, Moura FCC (2015) Magnetic amphiphilic nanocomposites based on silica-carbon for sulphur contaminant oxidation. New J Chem 39:5445–5452. doi:10.1039/C5NJ00593K

Pal N, Bhaumik A (2013) Soft templating strategies for the synthesis of mesoporous materials: inorganic, organic–inorganic hybrid and purely organic solids. Adv Colloid Interf Sci 189–190:21–41. doi:10.1016/j.cis.2012.12.002

Paździor K, Klepacz-Smółka A, Ledakowicz S, Sójka-Ledakowicz J, Mrozińska Z, Żyłła R (2009) Integration of nanofiltration and biological degradation of textile wastewater containing azo dye. Chemosphere 75:250–255. doi:10.1016/j.chemosphere.2008.12.016

Pinilla JL et al (2011) High temperature iron-based catalysts for hydrogen and nanostructured carbon production by methane decomposition. Int J Hydrog Energy 36:7832–7843. doi:10.1016/j.ijhydene.2011.01.184

Pizarro J et al (2015) Adsorption of Cu2+ on coal fly ash modified with functionalized mesoporous silica. Fuel 156:96–102. doi:10.1016/j.fuel.2015.04.030

Purceno AD, Barrioni BR, Dias A, da Costa GM, Lago RM, Moura FCC (2011) Carbon nanostructures-modified expanded vermiculites produced by chemical vapor deposition from ethanol. Appl Clay Sci 54:15–19. doi:10.1016/j.clay.2011.06.012

Putz A-M et al (2015) Pore ordering in mesoporous matrices induced by different directing agents. J Porous Mater 22:321–331. doi:10.1007/s10934-014-9899-z

Qin J, Li B, Zhang W, Lv W, Han C, Liu J (2015) Synthesis, characterization and catalytic performance of well-ordered mesoporous Ni-MCM-41 with high nickel content. Microporous Mesoporous Mater 208:181–187. doi:10.1016/j.micromeso.2015.02.009

Rahim Pouran S, Abdul Aziz AR, Wan Daud WMA, Embong Z (2015) Niobium substituted magnetite as a strong heterogeneous Fenton catalyst for wastewater treatment. Appl Surf Sci 351:175–187. doi:10.1016/j.apsusc.2015.05.131

Sing KSW, Everett DH, Haul RAW, Moscou L, Pierotti RA, Rouquerol J, Siemieniewska T (2008) Reporting physisorption data for gas/solid systems. In: Handbook of heterogeneous catalysis. Wiley-VCH Verlag GmbH & Co. KGaA. doi:10.1002/9783527610044.hetcat0065

Teixeira APC et al (2012) Iron: a versatile element to produce materials for environmental applications. J Braz Chem Soc 23:1579–1593

Vartuli JC et al (1994) Effect of surfactant/silica molar ratios on the formation of mesoporous molecular sieves: inorganic mimicry of surfactant liquid-crystal phases and mechanistic implications. Chem Mater 6:2317–2326. doi:10.1021/cm00048a018

Voss D (1999) Company aims to give fuel cells a little backbone. Science 285:683. doi:10.1126/science.285.5428.683

Wang Z et al (2015) Nanocarbons from rice husk by microwave plasma irradiation: from graphene and carbon nanotubes to graphenated carbon nanotube hybrids. Carbon 94:479–484. doi:10.1016/j.carbon.2015.07.037